Stability of Bacteriorhodopsin α-Helices and Loops Analyzed by Single-Molecule Force Spectroscopy

Daniel J. Müller,*† Max Kessler,‡ Filipp Oesterhelt,‡ Clemens Möller,* Dieter Oesterhelt,§ and Hermann Gaub‡
*Max-Planck-Institute of Molecular Cell Biology and Genetics, 01307 Dresden; †BIOTEC, Technical University Dresden, 01602 Dresden; ‡Center for Nano Science, Physics Section, Ludwig Maximilians University Munich, 80799 Munich; and §Max-Planck-Institute of Biochemistry, 82152 Martinsried, Germany

ABSTRACT The combination of high-resolution atomic force microscopy imaging and single-molecule force spectroscopy allows the identification, selection, and mechanical investigation of individual proteins. In a recent paper we had used this technique to unfold and extract single bacteriorhodopsins (BRs) from native purple membrane patches. We show that subsets of the unfolding spectra can be classified and grouped to reveal detailed insight into the individualism of the unfolding pathways. We have further developed this technique and analysis to report here on the influence of pH effects and local mutations on the stability of individual structural elements of BR against mechanical unfolding. We found that, although the seven transmembrane α-helices predominantly unfold in pairs, each of the helices may also unfold individually and in some cases even only partially. Additionally, intermittent states in the unfolding process were found, which are associated with the stretching of the extracellular loops connecting the α-helices. This suggests that polypeptide loops potentially act as a barrier to unfolding and contribute significantly to the structural stability of BR. Chemical removal of the Schiff base, the covalent linkage of the photoactive retinal to the helix G, resulted in a predominantly two-step unfolding of this helix. It is concluded that the covalent linkage of the retinal to helix G stabilizes the structure of BR. Trapping mutant D96N in the M state of the proton pumping photocycle did not affect the unfolding barriers of BR.

INTRODUCTION

Structure as well as dynamics, and thus the function, of biomolecules are determined by multiple inter- and intramolecular forces (Brooks et al., 1998; Haltia and Freire, 1995; Nakamara, 1996; White and Wimley, 1999). Such molecular interactions are typically inferred indirectly from equilibrium binding and kinetic measurements or are calculated with molecular models. With the development of single-molecule force spectroscopy such inter- and intramolecular interactions of biological macromolecules have become directly accessible. Consequently, this technique has been applied to measure interactions in proteins such as forces that mediate molecular recognition (Fritz et al., 1998; Lee et al., 1994; Moy et al., 1994), stabilize molecular structures (Fisher et al., 1999; Rief et al., 2000), and drive intermolecular interactions (Dammer et al., 1996), molecular bonds (Grandbois et al., 1999; Merkel 2001), and molecular elasticities (Bustamante et al., 2000; Clausen-Schaumann et al., 2000; Kellermayer et al., 1997; Rief et al., 1999, 1998a). Modular proteins were unfolded and revealed for the first time a direct correlation between folding pattern and mechanical function. Models were developed that allow a theoretical description of the molecular compliances based on the combination of established polymer models in combination with discrete unfolding events (Rief et al., 1998a; Zhang et al., 1999). Forced unfolding experiments performed on fibronectin (Rief et al., 2000), tenascin (Oberhauser et al., 1998), and titin (Oberhauser et al., 1999; Rief et al., 2000), showed these modular proteins to unfold domain after domain but only in an all-or-none event with no intermediate states. Only in rare cases have intermittent steps been reported recently (Marszalek et al., 1999).

Because all these mechanical unfolding experiments had been performed on either modular proteins or tandem constructs of multiple domains, the assignment of a certain unfolding event to a certain domain was not possible: the weakest domain unfolds first, not the first in the chain. We could overcome this limitation by unfolding membrane proteins. The highest resolution was obtained with bacteriorhodopsin (BR). Here individual structural elements of the protein were found to unfold sequentially, which made the assignment of certain features of the measured force spectra to the corresponding amino acid (aa) sequence possible. Such spectra then provided detailed information on structural properties of individual BR molecules within the native purple membrane from the halophilic archaeon *Halobacterium salinarum* (Forbes and Lorimer, 2000; Oesterhelt et al., 2000).

The light-driven proton pump BR was chosen as model system for this study because it represents one of the most extensively studied membrane proteins (Haupts et al., 1999; Oesterhelt, 1998). BR converts the energy of light (λ = 500–650 nm) into an electrochemical proton gradient, which in turn is used for ATP production by the cellular ATP synthase. Its structural analysis has revealed the photoactive retinal embedded in seven closely packed trans-

Submitted January 16, 2002, and accepted for publication July 29, 2002.

Address reprint requests to Dr. Hermann E. Gaub, Center for Nano Science, Sektion Physik, Ludwig Maximilians-Universität München, Amalienstrasse 54, 80799 München, Germany. Tel.: 49-89-2180-3173; Fax: 49-89-2180-2050; E-mail: gaub@physik.uni-muenchen.de. or to Dr. Daniel Müller, BiOTEC, 01307 Dresden, Germany. Tel.: 49-351-210-2586; Fax: 49-351-210-2020; E-mail: mueller@mp1-6BG.DE.

0006-3495/02/12/3578/11 $2.00

membrane α-helices (Belrhali et al., 1999; Essen et al., 1998; Grigorieff et al., 1996; Luecke et al., 1999; Mitsuoka et al., 1999), which builds a common structural motif among a large class of related G-protein-coupled receptors (Baldwin, 1993; Helmreich and Hofmann, 1996; Kolbe et al., 2000; Palczewski et al., 2000; Royant et al., 2001). The BR helices are lettered A, B, C, D, E, F, and G, to which the C-terminal end is connected. With increasing knowledge of its structural and functional properties, BR has become a paradigm for α-helical membrane proteins in general and for ion transporters in particular (Lanyi, 1999). Together with adjacent lipids BR molecules assemble into trimers, which are packed into a two-dimensional hexagonal lattice of the purple membrane as a chemically distinct domain of the cell membrane.

In this study we measure the unfolding spectra of BR by high-resolution atomic force microscopy (AFM) imaging and single-molecule force spectroscopy. In extension of our previous work we improved and expanded the experimental and data analysis procedures. To test whether drastic changes of the physiological conditions influence the stability, wild-type BR was unfolded within a pH range from 4.2 to 10. Subsequent analysis of the unfolding spectra in combination with the classification of individual force peaks provided a detailed insight into the stability and the unfolding steps of BR's secondary structural elements. To elucidate the influence of retinal and its different configurations on the folding potential we additionally unfolded photobleached BR and the D96N BR mutant trapped in the M state of the photocycle.

MATERIALS AND METHODS

Purple membrane preparation

Wild-type purple membrane was extracted from *H. salinarum* as described (Oesterhelt and Stoeckenius, 1974) and adsorbed onto freshly cleaved mica (Müller et al., 1997). The cystein mutant (G241C) has been created by recombinant techniques replacing the glycine at position 241 with a cysteine as described (Pfeiffer et al., 1999). The BR D96N mutant showing a significantly retarded photocycle has been created by replacing the aspartic acid at position 96 with asparagine and characterized by spectroscopic methods as described (Butt et al., 1989; Holz et al., 1989). During the unfolding of the D96N mutant it was illuminated with sufficient yellow light intensity ($\lambda = 475$ nm; filtered from a 75-W halogen lamp, with heat filter focused on a spot of 5 cm) to trap the BR molecules in the M state of the catalytic cycle. Controlled photobleaching of purple membranes (10 μg/ml) was performed in the presence of 200 mM hydroxylamine (pH 7.2, 20 mM Tris-HCl) as described (Möller et al., 2000; Oesterhelt et al., 1974).

Attachment of BR to the AFM tip

In previous studies, two different strategies have been developed to attach the protein to the tip. In a recent paper we showed that the cysteine of the G241C mutant binds with a 90% likelihood to a gold-coated cantilever (Oesterhelt et al., 2000) when the tip is brought into contact with the cytoplasmic purple membrane surface even at forces below 200 pN. This procedure allows for a highly efficient and well localized attachment. However, it requires the AFM tip to be replaced after a few experiments because it is covered with reacted protein. The alternative method, the nonspecific attachment in combination with a subsequent imaging and force trace classification, was shown to provide equivalent results; however, it allows a much higher throughput. Because this study here is a systematic investigation, we chose the nonspecific attachment in combination with AFM imaging as described below.

Single-molecule force spectroscopy and imaging

The contact mode AFM (Nanoscope E, Digital Instruments, Santa Barbara, CA) used was equipped with a 100-μm piezo scanner. The spring constants k of the 100-μm-long Si_3N_4 AFM cantilevers (OMCL TR400PS, Olympus, Tokyo, Japan) were calibrated in solution after the experiments using the equipartition theorem (Butt and Jaschke, 1995; Florin et al., 1995). Within the uncertainty of this method (~10%) all cantilevers used exhibited the same $k = 0.1$ N/m. All experiments were done in buffer solution (300 mM KCl, 10 mM Tris-HCl, and unless noted otherwise, pH 7.8) at room temperature. To perform force spectroscopy experiments on BR we recorded topographs of the cytoplasmic purple membrane surface (Müller et al., 1999b) at sub-nanometer resolution as described (Müller et al., 1999a). After this, we selected an area of BR trimers and zoomed in, positioning the AFM tip. To allow the C-terminal end of BR to adsorb onto the tip, both were kept in contact for ~1 s while applying a force of 0.5–1 nN. The AFM stylus and protein surface were then separated at a velocity of 40 nm/s while recording the force spectrum. In ~15% of all retraction curves we detected an adhesive peak, which was correlated to a removal of a single BR molecule, and ~30% of these adhesion curves showed a force extension curve exhibiting a length between 60 and 70 nm (see data analysis). After detecting one discontinuous force curve the protein surface of the same area was re-imaged. Defects of missing BR monomers allowed us to unambiguously correlate the force spectra to a single protein. Fig. 1 shows the image of a purple membrane before (Fig. 1 *b*) and after (Fig. 1 *c*) extraction of a single BR (note the persistent defect in both images).

Data analysis

To analyze the force curves, a clear criterion is required that distinguishes curves of BR molecules attached to the AFM tip with different regions of their polypeptide backbone. One suitable criterion is the overall length of the force curve, which reflects the tip-sample distance at which the last force peak occurs. It is evident that a molecule attached to the cantilever by one of its loops results in a force curve with smaller overall length than a molecule attached by one of its termini. If the AFM tip binds to the EF loop, the force adhesion curve could exhibit a maximum length of ~152 aa. The maximal length of the stretched polypeptide chain (152 aa) was calculated assuming attachment to the EF loop (aa 157–164 as derived from the atomic model of BR) and that the extracellular N-terminal end forms the last potential barrier against extraction of BR from purple membrane. Stretching 152 aa, at an approximate force of 200 pN, corresponds to a maximum rupture length of ~48 nm, calculated using the worm-like chain (WLC) model. Taking this approach, the maximum rupture length of the unfolded BR molecule would be 92 aa (~29 nm) if the tip binds to the CD loop and 158 aa (~50 nm) if the tip binds to the AB loop (here the last potential barrier would be built by the G-helix). Some of the adhesion peaks of these curves would then represent simultaneous pulling on two secondary structural elements, each of them connected to one end of the polypeptide loop. Thus, in most cases the classification and analysis of such concurrent multiple unfolding events cannot be made ambiguously. The classification of force curves exhibiting a length of ~50 nm was further complicated by the partial unfolding of BR molecules that attached via their C-terminal end to the tip. Such analytical problems do not occur when the protein is fully unfolded, beginning from the C-terminal end. Force-extension curves corresponding to an extension of significantly

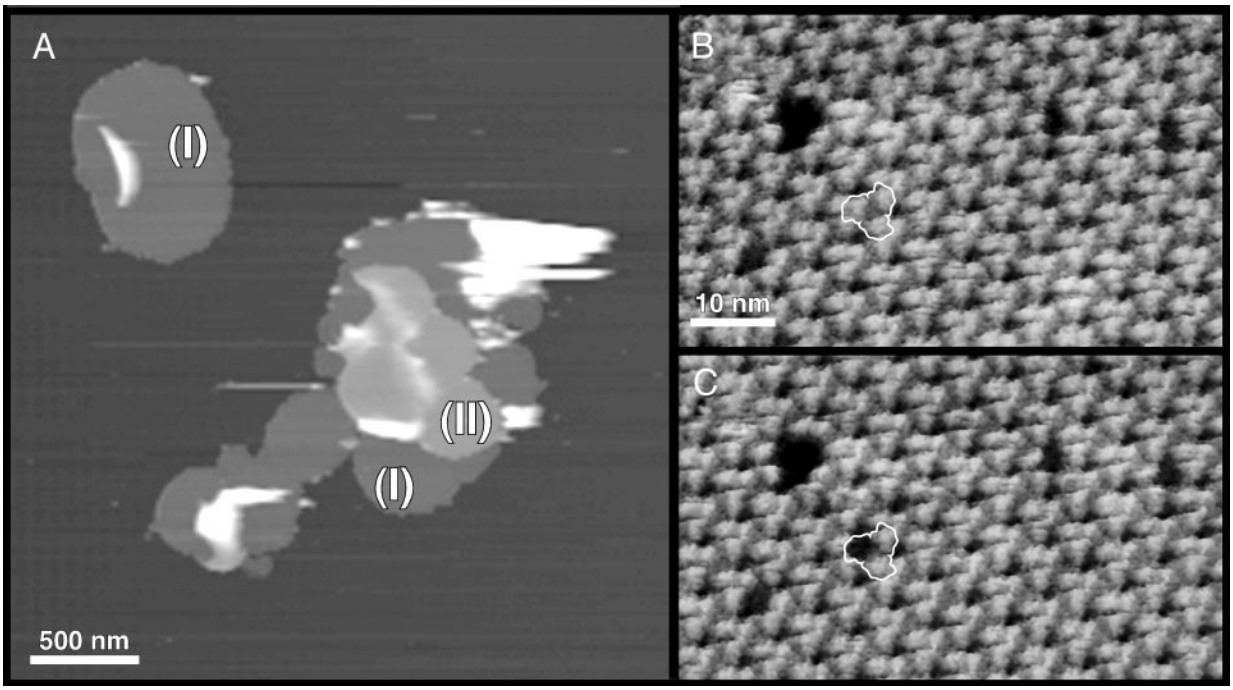

FIGURE 1 Purple membrane imaging and manipulation. (*a*) Purple membrane patches (*I*) adsorbed onto freshly cleaved mica and imaged in buffer solution (pH 7.8, 20 mM Tris-HCl, 300 mM KCl). In some areas, purple membrane patches overlap with other membranes, forming double layers (*II*). (*b*) High-resolution image of the cytoplasmic purple membrane surface showing BR trimers (*outline*) arranged into a hexagonal lattice. The topograph was recorded at minimum force allowing the longest cytoplasmic loops of the individual BR molecules (loop EF) to protrude fully from the membrane surface (Müller et al., 1999b). Individual defects show single or multiple BR monomers missing. After imaging, the AFM tip was brought into contact to the membrane surface (*circle*). This allowed the polypeptides of individual BR molecules to adsorb to the tip. During separation of tip and sample, this molecular bridge was used to pull on the protein, and the force spectrum was recorded (see Fig. 2). (*c*) Same purple membrane area imaged after the manipulation shows one individual BR monomer missing (*circle*). Vertical full gray levels of topographs correspond to 50 nm (*a*) and 1.2 nm (*b* and *c*).

more than 158 aa (~50 nm) can result only from attaching the C-terminal end to the tip. Therefore, only those force-extension curves exhibiting a length above 60 nm were selected and analyzed. This stringent criterion ensured that all the analyzed curves belonged to the same subset, thus allowing a detailed analysis to be made.

By selection of the force-extension curves exhibiting an overall length between 60 and 70 nm we were sure to analyze only spectra from BR molecules that were attached by their C-terminus to the AFM tip and that were completely elongated during extraction (Oesterhelt et al., 2000). All force curves exhibiting these overall lengths were selected and aligned at the second main peak at a tip-to-purple membrane separation of ~27 nm (Fig. 2). The force curves were aligned at the second main peak because the curves showed offsets in the distance between stylus and purple membrane (Fig. 2; region around 0 nm). The main reason for this offset is that principally every amino acid of the C-terminal can bind to the AFM tip and that the point of contact is not necessarily located at the tip apex but can also occur at the side of the tip. Avoiding statistical difficulties we analyzed only relative positions of the peaks. We used identical procedures and criteria to align each data set.

To analyze the side peaks, however, we superimposed every main peak separately (see Figs. 3–6 and 8). Every single peak of these superimpositions was fitted by the WLC model with a persistence length of 4 Å (Rief et al., 1997a) and a monomer length of 3.6 Å. We calculated the number of unfolded aa at each peak using the contour length as obtained from the WLC model. When pulling the polypeptide from the cytoplasmic surface, the anchor of the peptide sometimes had to be assumed to exist at the opposite, extracellular surface. In this case, the membrane thickness (~4 nm) had to be considered, and 11 aa (11×3.6 Å ≈ 4 nm) were added to the number of aa determined by the WLC model. This allowed calculating the entire rupture length of the unfolded polypeptide. To compare the polypeptide length derived from the WLC fits with the BR structure we have chosen the atomic model of Mitsuoka et al. (1999).

RESULTS AND DISCUSSION

Protein extensibility

With state-of-the-art AFM or, if higher force resolution is required, with force spectroscopy equipment (Oesterhelt et al., 1999; Rief et al., 1997b), the extensibility of molecules can be measured by stretching the molecule that is attached to the AFM tip and recording the cantilever deflection while increasing the cantilever sample distance. The deflection is converted into a force by multiplication with the spring constant, which is determined for each cantilever by the thermal fluctuation method (Butt and Jaschke, 1995; Florin et al., 1995). By subtracting the cantilever's deflection from the tip-sample distance for each point of the measurement, the so-called force-extension traces are calculated.

Fig. 2 shows a multitude of force-extension traces, each one recorded on one single BR (such as shown in Fig. 1), exhibiting a richness of detailed information on the mechanics of this molecule. In these figures ~25 traces are superposed and plotted. This kind of graphic representation high-

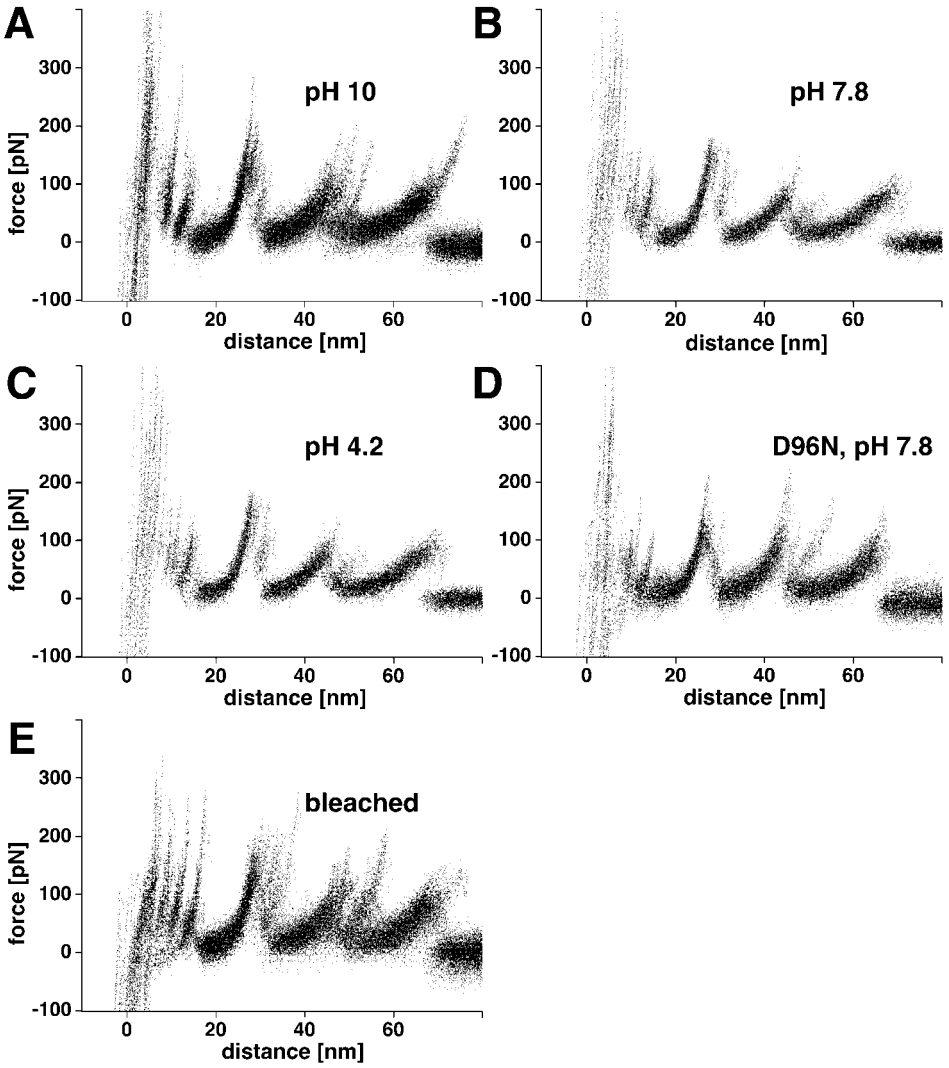

FIGURE 2 Unfolding BR at various conditions. To show common unfolding patterns among single-molecule events, the force spectra were superposed. (*A–C*) BR unfolded at pH 10 ($n = 31$), pH 7.8 ($n = 32$), and pH 4.2 ($n = 20$), respectively. (*D*) BR mutant D96N ($n = 18$) unfolded at pH 7.8. During recording the force spectra the mutant was illuminated with yellow light ($\lambda = 475$ nm), thereby trapping the M state of the photocycle. (*E*) BO unfolded at pH 7.8 ($n = 29$). BO was formed after cleaving the covalent retinal bond (Schiff base) using hydroxylamine. Temperature (21°C) and electrolyte concentration (300 mM KCl) were kept constant in all experiments. All molecules were unfolded by grabbing the C-terminus at the cytoplasmic surface (Oesterheltet al., 2000). The force curves recorded on native purple membrane (*A–D*) exhibited a SD of 9.6 pN ($n = 20$) whereas those recorded on the apo-membrane (*E*) exhibited a SD of 12.9 pN ($n = 20$).

lights common features through the accumulation of the measured points and at the same time represents the individualism of traces. The individualism of the traces is dealt with in Figs. 3–8. The common feature of all the traces is that upon stretching the force builds up in a gradual but nonlinear fashion until at a certain force the trace drops abruptly to lower forces before it rises again upon further extension. Beyond an extension of 70 nm no interaction force is measured. To exclude that the membrane bending contributed to the force spectra we compared force extension curves recorded on purple membranes of different sizes and on different areas of the membrane (e.g., center or outer rim) itself. Apparently, the force curves showed no differences, indicating such effects to be negligible.

In previous studies we learned that unfolded proteins behave in a first approximation like random coils whose elasticity is well described by the WLC model with an apparent persistence length of 4 Å (Rief et al., 1997a). It should be noted here that this apparent persistence length includes also enthalpic contributions to the molecular elasticity, which become apparent at higher forces (Bouchiat et al., 1999; Oesterhelt et al., 1999; Rief et al., 1998b). The gradual, nonlinear force increase in the extension traces can be well fitted with the WLC model with only one free

parameter: the contour length of the stretched portion of the molecule. As seen in Figs. 3-6 and 8 this fit describes the increasing slopes of the traces at low forces with good agreement. At higher forces the deviations are sometimes marked, indicating that additional processes occur.

From these fits we conclude that in the region of increasing force we stretch an unfolded protein backbone until at a certain force the tension drops suddenly. Because the force builds up again upon further stretching (except for the last peak) we interpret this drop as the extraction of another segment of the protein from the membrane. Upon extraction this segment unfolds, and because the unfolded configuration is less compact, the additional contour length of the freely fluctuating protein backbone results in a drop of the entropically dominated restoring force of the protein.

The WLC fit of the rising slope of the peaks thus provides the contour length of the unfolded protein and by means of this the position of the corresponding barrier against unfolding. With the known attachment point of the protein to the AFM tip, the position of this barrier with respect to the aa sequence of the backbone can thus be counted backwards from the C-terminus. Based on the well established structure of BR, we then can, at least in principle, assign for each peak the corresponding aa in the folded protein, which marks the transition point to the unfolded portion of the protein. The force, which under the given experimental conditions is required to overcome this barrier, is given by the height of the peak.

In previous studies we and others have shown that unfolding forces are rate dependent and that additional information on the geometry of the potential barriers may be extracted from the unfolding traces by varying the pulling speed (Heymann and Grubmüller, 2000; Merkel et al., 1999; Rief et al., 1998a). We have not yet exploited this potential in this study. Because all the conclusions drawn here are based on length arguments rather than forces, our conclusions are independent of the pulling speed.

In summary, each adhesion peak of the discontinuous force spectrum marks a potential barrier of the BR molecule whose position is determined by a WLC fit.

Unfolding traces of BR

Fig. 2 shows five panels of BR unfolding traces recorded under different conditions. In all traces the gross features are alike, with systematically differing details (Figs. 3–8). In a previous study (Oesterhelt et al., 2000), we already had assigned the main peaks to different processes: the peaks below 20 nm include unfolding of helices G and F. At 27, 45, and 65 nm, helices E and D, B and C, and A unfold, respectively. Whereas these main peaks remain more or less unaltered for all the different conditions, the side peaks vary significantly. These side peaks therefore merit detailed analysis.

It is the major benefit of single molecule experiments that each experiment with each molecule may be analyzed individually. This unique option allows the discrimination between the molecules as individuals (be it temporarily or persistently in a different state) as well as between different pathways, which the individual experiments follow. Based on the analysis of each unfolding trace the traces may be sorted and grouped according to certain criteria. Because the effort is enormous, we performed this task for only one pH value per block. All blocks were analyzed for pH 4.2 except for the data in Figs. 3 and 8, which were recorded at pH 7.8 to be comparable with the M state data in Fig. 2 *D*. The result is depicted in Figs. 3–6 and 8.

Mutant D96N was investigated to elucidate the influence of the intermediate (M) state conformation of BR on the unfolding pattern. As can be seen by the direct comparison between Fig. 2 *D* with the other traces, no significantly marked changes occur whether BR was trapped in the M state of the photocycle or not.

Unfolding helices G and F

The low extension part, below 30 nm, of all traces superimposed in Fig. 2 *B* was analyzed individually. Three different main groups became apparent that were superimposed in Fig. 3, *a–c*. The first group of traces exhibited only the 36-aa peak (Fig. 3 *a*). In a second group an additional peak at 48 aa occurred with slightly higher probability (Fig. 3 *b*). Only a very minor fraction exhibited a peak at ~26 aa (Fig. 3 *c*), which will be discussed below in connection with the apoprotein. The peaks below 5 nm could not be ordered in any systematic way. We interpret them as the stretching of the C-terminus. Their variation in position reflects the different attachment sites of the molecule at the tip and thus the length variation of the freely fluctuating segment of the chain. The schematic in Fig. 3 depicts the model that corresponds to the measured positions of the barriers. According to this model the sequence of the extraction/unfolding process is as follows. First the free C-terminal chain is stretched and then helix G unfolds. Then the force acts on the GF loop (peak at 36 aa), and in ~65% of the traces this loop is stretched and pulled through the membrane resulting in the peak at 48 aa (Fig. 3 *b*). Alternatively, the loop may be extracted together with helix F so that this peak is skipped (Fig. 3 *a*), and the force starts rising only when it acts directly on helix E. The forces that are required to overcome both barriers are both ~100 pN, the first one slightly higher than the second.

Unfolding helices E and D

The trace segments of Fig. 2 *C*, showing interactions separated between 15 and 40 nm from the membrane surface,

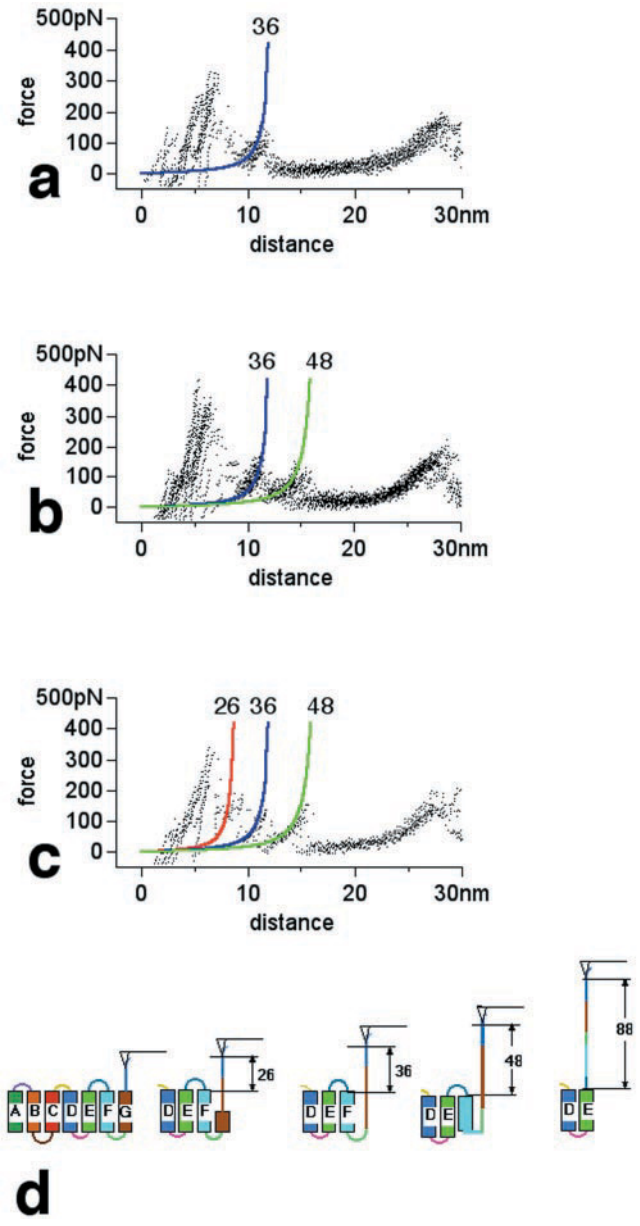

FIGURE 3 Unfolding pathways of transmembrane α-helices G and F. (*a*) Unfolding helices G and F in two steps. After unfolding helix G the polypeptide chain, bridging the AFM tip and purple membrane, exhibits a length of 36 aa (blue fit). The loop connecting helices G and F remains at the opposite, extracellular surface, and helix F remains embedded in the membrane. The latter two structures and the loop connecting helices E and F are unfolded within a single step, exceeding a force of 111 ± 34 pN (n = 10). (*b*) Unfolding of helices G and F and their connecting loop in a three-step process. First, helix G is unfolded, increasing the length of the stretched polypeptide to 36 aa (blue fit). Then, the hydrophilic GF loop is pulled into the hydrophobic membrane (at 124 ± 28 pN), and the stretched polypeptide then exhibits a length of 48 aa (green fit). After this, helix F and the cytoplasmic loop connecting helices F and E are unfolded in a single step at forces ≥110 ± 32 pN (n = 17). (*c*) Helices G and F and loop GF unfold in a four-step process. The first part of helix G is unfolded to the approximate retinal location, which forms an internal potential barrier (red fit). The polypeptide is stretched again, and what remains of helix G is unfolded at 148 ± 36 pN, increasing the stretched polypeptide length to 36 aa (blue fit). After this, the FG loop is pulled into the membrane (at 102 ± 44 pN), increasing the length to 48 aa (green fit). Finally, helix F and the loop connecting helices F and E are unfolded in a single step at 102 ± 31 pN (n = 5). (*d*) Schematic drawing of the unfolding pathways of helices G and F and of loop FG. All unfolding events were fitted using the WLC model as described in Materials and Methods. The total number of force curves shown corresponds to 32.

were analyzed accordingly. Here we found four distinctly different groups of traces that are depicted in Fig. 4.

In the simplest case, which accounts for ~22% of all traces, one peak at 88 aa is seen (Fig. 4 *a*). Our only explanation for this finding is that helices E and D both unfold in an all-or-none event together. In ~12% of the cases we find an intermittent peak at 94 aa, which reflects a barrier around aa 154 of BR (derived from 248–94 aa; Fig. 4 *b*). In 45% of the traces we find a peak at 105 aa (Fig. 4 *c*), which, based on the model (Fig. 4 *e*), corresponds to a state where helix E is completely unfolded, but helix D is still intact. Approximately 20% of the traces show all three peaks (Fig. 4 *d*), which means that the BR molecules measured here went through both intermittent states upon unfolding. The peak heights were ~160 pN for the first two barriers and significantly lower for the third (90 pN). The most striking feature of this set is the potential barrier in the proximity of aa 154 of BR.

Unfolding helices C and B

In the length window between 35 and 55 nm we found again four different groups of traces (Fig. 5). The majority of the traces exhibited no extra peak between148 and 220 aa, indicating a simultaneous unfolding of helices B and C. A minor fraction of the traces (9%) showed an additional peak at 158 aa (Fig. 5 *b*) and 35% a second peak at 175 aa (Fig. 5 *c*). The first case would fit to the extracellular BC loop still untouched, whereas in the second case this loop is completely stretched. In both cases helix B is intact. In 10% of the traces we find all three peaks (Fig. 5 *d*), indicating that both intermittent states are visited on the unfolding pathway. All peaks are ~100 pN in height.

Unfolding helix A

In 65% of the traces the last peak (Fig. 6) occurs at 65 nm, corresponding to a stretched unfolded polypeptide of 220 aa in length (Fig. 6 *a*). In these traces the last helix is pulled out of the membrane in a single step at forces of ~100 pN. In the other cases, a second peaks follows (Fig. 6 *b*). This second peak is smeared out considerably, and the rupture point varies. Drawn in blue is the WLC fit for the fully stretched length of 232 aa from BR. Because this last peak also occurs on multilamellar membrane stacks (see discussion below) it must reflect the destabilization of the N-

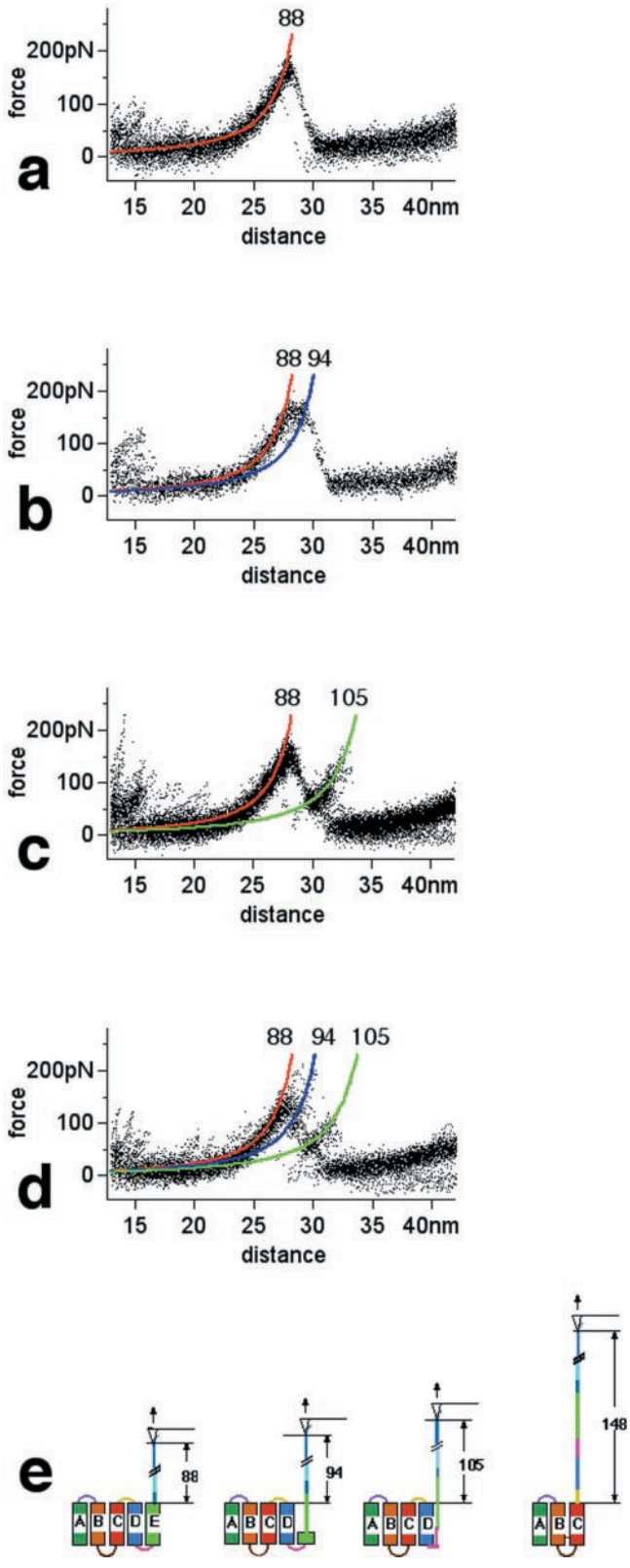

FIGURE 4 Unfolding pathways of transmembrane α-helices E and D. After unfolding helices F and G, the polypeptide chain, bridging the AFM tip and purple membrane, exhibits a length of 88 aa (red fit). All other helices remain embedded in the purple membrane. (*a*) The structural motif of helices E and D, loop ED, and loop DC unfold in a single step upon exceeding an average pulling force of 167 ± 20 pN (n = 20). (*b*) Helices E and D unfold in a two-step process. First, helix E unfolds partly (at 169 ± 22 pN), thereby lengthening the stretched polypeptide to 94 aa (blue fit). After this, the force pulls the remaining part of helix E and, on the hydrophilic loop, connecting helices E and D located on the opposite, extracellular surface. Upon exceeding an average pulling force of 169 ± 21 pN, the remaining part of helix E, the loop ED, helix D, and the cytoplasmic loop CD are unfolded simultaneously (n = 10). (*c*) Helices E and D unfold in an alternate two-step process. First, part of helix E and the loop ED connecting both helices unfold at 161 ± 14 pN, thereby lengthening the stretched polypeptide to 105 aa (green fit). Upon exceeding an average pulling force of 86 ± 23 pN, helix D and loop CD are unfolded (n = 39). (*d*) Helices E and D and loop ED unfold in a three-step process. First, part of helix E unfolds at 152 ± 22 pN, thereby lengthening the stretched polypeptide to 94 aa (blue fit). Second, what remains from helix E and loop ED is pulled into the membrane at 135 ± 30 pN, lengthening the polypeptide strand to 105 aa (green fit). Third, helix D and loop CD unfold at a pulling force above 83 ± 23 pN (n = 19). (*e*) Schematic drawing of the unfolding pathways found. The total number of force curves shown corresponds to 88.

terminus, its possible interaction with the neighboring proteins, and the pulling through the hydrophobic membrane.

Stability of the loops

One remarkable finding of this study is the measured potential barrier associated with the N-terminus and the extracellular loops connecting the transmembrane α-helices. To exclude adhesion of the loops to the mica surface as a potential explanation we performed the same experiments on the upper membrane of double-layered purple membrane patches (compare Fig. 7) like the ones shown in Fig. 1 and of purple membrane adsorbed onto hydrophobic graphite (data not shown). In both cases, we did not observe a change in the adhesion peak positions and distributions. Because it would be highly unlikely that a hypothetic adhesive interaction of the loops with mica is the same as with another purple membrane or with graphite, we conclude from these experiments that the loops are stable structural elements. Thus, a potential barrier comparable with the one that is associated with the unfolding of the α-helices needs to be overcome to stretch the loops and to pull them through the membrane. Interestingly, these forces required to overcome the barriers do not depend in an obvious way on the length of the loop (i.e., 102 pN for loop GF, 4 aa; 135 pN for loop ED, 3 aa; and 109 pN for loop CB, 17 aa). This indicates that the process is dominated by an activation barrier. Because these forces are on the order of 100 pN, the width of these barriers must be far less than the thickness of the membrane to be compatible with measured unfolding free energy changes. This again speaks for a breakup of a structure. On the other hand, x-ray and electron diffraction studies on crystallized BR shows these loops to exhibit a well defined structural conformation. The B-factors and temperature factors of the BR structures are similar for all

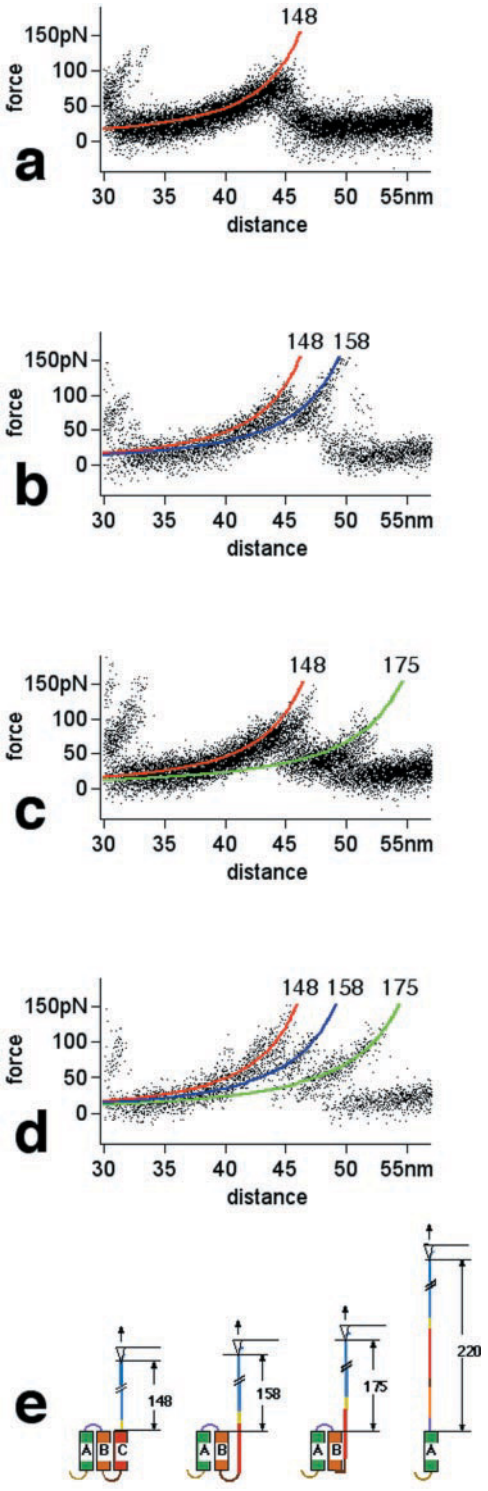

FIGURE 5 Unfolding pathways of transmembrane α-helices C and B. After unfolding helices E and D, the polypeptide chain, bridging the AFM tip and purple membrane, exhibits a length of 148 aa (red fit). Helices C, B, and A remain embedded in the purple membrane. (*a*) Helices C and B unfold in a single step upon exceeding an average pulling force of 99 ± 16 pN (n = 40). (*b*) Helices C and B unfold in a two-step process. First, helix C unfolds at 109 ± 18 pN, thereby lengthening the stretched polypeptide to 158 aa (blue fit). After this, the force pulls on the hydrophilic loop connecting helices C and B located on the opposite, extracellular surface. Upon exceeding an average pulling force of 105 ± 15 pN, the extracellular loop BC, helix B, and the cytoplasmic loop AB are unfolded simultaneously (n = 8). (*c*) Helices C and B unfold in an alternate two-step process. First, helix C and the loop connecting these helices unfold at 95 ± 20 pN, thereby lengthening the stretched polypeptide to 175 aa (green fit). Upon exceeding an average pulling force of 80 ± 17 pN, helix B and loop AB are unfolded (n = 31). (*d*) Helices C and B unfold in a three-step process. First, helix C unfolds at 108 ± 26 pN, thereby lengthening the stretched polypeptide to 158 aa (blue fit). Second, loop BC is pulled into the membrane at 116 ± 33 pN (green fit). Third, helix B unfolds at pulling forces above 87 ± 31 pN (n = 9). (*e*) Schematic drawing of the unfolding pathways found. The total number of force curves shown corresponds to 88.

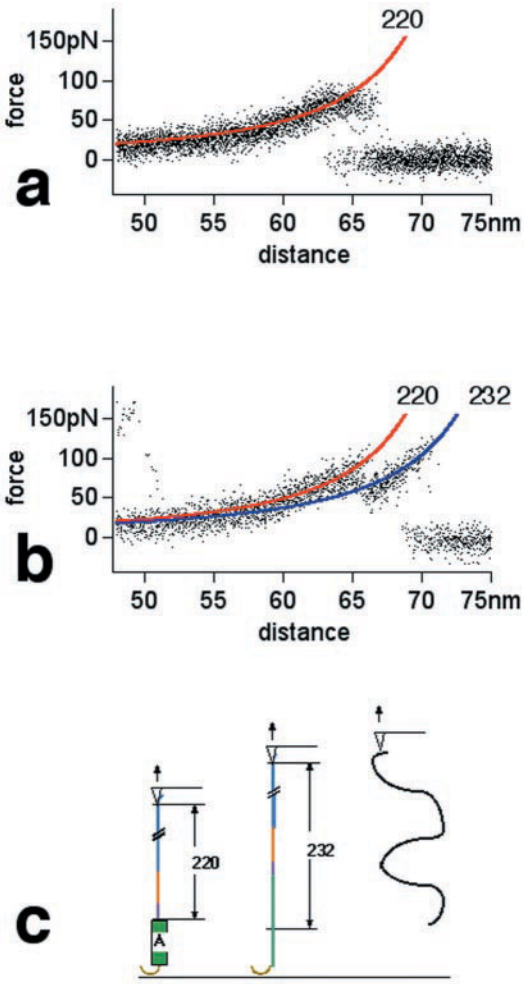

FIGURE 6 Unfolding pathways of the transmembrane α-helix A. After unfolding helices C and B, the polypeptide chain, bridging the AFM tip and purple membrane, exhibits a length of 220 aa (red fit). Only helix A remains embedded in the membrane. (*a*) Helix A and the N-terminal end are pulled through the membrane within a single step at average pulling force of 87 ± 9 pN (n = 12). (*b*) Helix A unfolds at 99 ± 11 pN, and the N-terminal end anchors the polypeptide (n = 6). The length of the stretched polypeptide corresponds to 232 aa (blue fit). After this, the force pulls on the hydrophilic N-terminus located on the opposite, extracellular surface. By exceeding a pulling force of 105 ± 11 pN, the polypeptide end is pulled through the membrane. (*c*) Schematic drawing of the unfolding pathways found. The total number of force curves shown corresponds to 18.

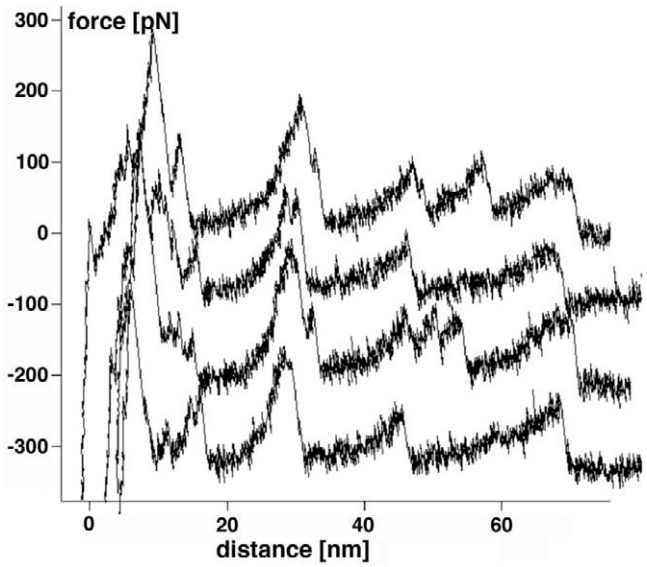

FIGURE 7 Unfolding BR on double-layered purple membrane. To show that the common unfolding patterns of BR do not depend on interactions with the supporting mica surface, single BRs of double-layered purple membranes were unfolded at pH 7.8, 300 mM KCl. Although only a few force curves were shown, their traces show almost all the unfolding pathways described in Figs. 3–6.

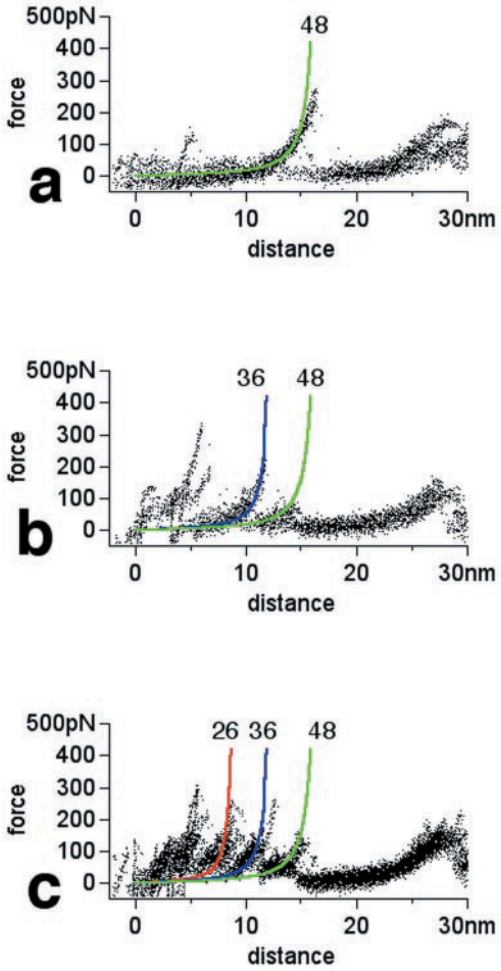

FIGURE 8 Transmembrane α-helices F and G of BO prefer different unfolding pathways compared with native BR. (*a–c*) Events are described by similar pathways as those shown in Fig. 3, *a–c*, respectively. In contrast to BR, however, BO prefers the four-step unfolding pathway shown in *c*. Adhesion forces and frequencies were 189 ± 56 pN ($n = 6$) in *a*; 113 ± 64 pN (blue fit) and 61 ± 13 pN (green fit) at $n = 6$ in *b*; and 122 ± 41 pN (red fit), 130 ± 61 pN (blue fit), and 124 ± 58 pN (green fit) at $n = 17$ in *c*. The total number of force curves shown corresponds to 29.

extracellular loops and the transmembrane α-helices, indicating that they exhibit equally high conformational stability (Belrhali et al., 1999; Essen et al., 1998; Luecke et al., 1999; Mitsuoka et al., 1999). This finding was also confirmed by experiments determining the solution structure of truncated BR loops, which showed conformations close to those observed on intact BR (Katragadda et al., 2000).

Adsorbed to an atomically flat surface, lipid membranes can be assumed to be separated by an ~1-nm-thick water layer (Sackmann, 1996). A water layer of similar thickness can be assumed to separate purple membrane adsorbed to the mica surface or even to exist between stacked purple membranes. Such thin water layers, however, exhibit different properties compared with water of the bulk solution and behave more as a gel-like material. This effect may also influence the surface structures of BR as detected by the enhanced stability in our experiments.

Apo-membrane

Bulky side groups like tyrosine are possible candidates establishing helix-breaking regions. Thus, it can be assumed that such side groups may also divide the unfolding barriers of transmembrane α-helices. Which role does the retinal moiety play with respect to this aspect? Illuminating BR in the presence of hydroxylamine is known to cleave off the retinal, which is covalently attached through the Schiff base to Lys216 (Oesterhelt et al., 1974). The photobleaching reaction of BR yields the apoprotein bacterio-opsin (BO) and retinaloxime.

A comparison of Fig. 2 *B* (BR) with Fig. 2 *E* (BO) reveals that only minor changes in the force traces have occurred after cleavage of the retinal. The only significant change occurred in the area of the GF peaks. A direct comparison between these areas in Fig. 3 (BR) and Fig. 8 (BO) shows that the peak at 26 aa, which was negligible in BR, is now prominent in BO (Fig. 8 *c*). Although small, the average forces of the detected peaks were three times larger compared with the standard deviation of the noise (~13 pN). The probability distribution of the unfolding pathways of helices G and F is shown in Fig. 9. The probability of potential barriers occurring simultaneously at 26 and 48 aa decreased from 53% (BR) to 21% (BO), whereas the prob-

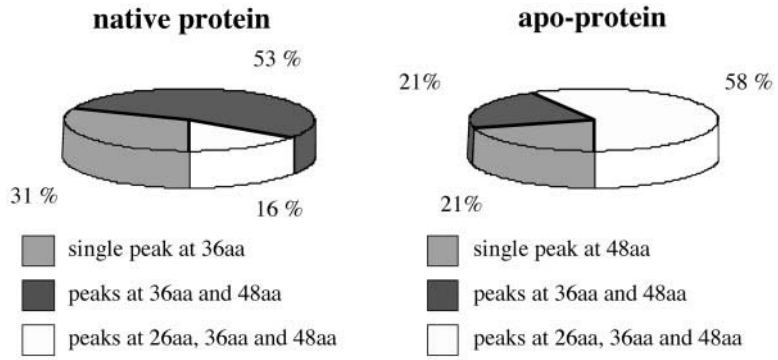

FIGURE 9 Probability distribution of pathways detected upon unfolding helices G and F. Probability of the unfolding pathways are shown for native BR (Fig. 3) and for the apoprotein (Fig. 8). Although 58% of the unfolding events of apoprotein showed an additional unfolding barrier at 26 aa, this barrier was observed in only 16% of the unfolding traces of wild-type BR.

ability of potential barriers occurring simultaneously at 26, 36, and 48 aa increased from 16% (BR) to 58% (BO). Correlation with the secondary structural model of BR shows that the additional peak fitted at 36 aa can be assigned to the position of the Schiff base of helix G to which the retinal is bond. It is counterintuitive, but the removal of this rather bulky retinal from the aa backbone results in the formation of an additional barrier in the unfolding pathway. However, the results indicate that the breakage of the Schiff base, which covalently links the retinal to helix G, destabilizes this α-helix.

Concluding remarks

It is the combination of high-resolution imaging with single-molecule force spectroscopy that has enabled us to record and unambiguously identify force traces from individual protein unfolding events. The one-by-one analysis of these unfolding traces allowed us to unravel correlations between the individual events and to discover distinct unfolding patterns, which led to a classification of the different unfolding pathways. There exists, however, a common unfolding principle of the BR structure in which a structural element is described by two transmembrane α-helices connected by their polypeptide loop. In most experiments, these three structural elements unfold within a single step. Some unfolding traces show these structural elements to choose separate unfolding pathways. As a result, every helix and the connecting loop are unfolded in a single step. In most cases, the second helix of this structural motif unfolds at smaller forces compared with the first helix. Most probable, this effect results from the destabilization of the structural motif by the unfolding process. The individualism of the unfolding pathways emerged as a very prominent feature throughout the study. Whether or not this individualism of the pathways reflects the individualism of the proteins remains to be decided in future studies. Although we have quite precisely measured the positions of the different unfolding barriers, we have not yet identified their underlying mechanisms. Particularly, our finding that the extracellular loops resist unfolding with a force that is comparable to the force required to unfold a transmembrane α-helix will require additional future investigations.

We thank Harald Janovjak and Matthias Rief for stimulating discussions. This work was supported by the Volkswagenstiftung and the German Science Foundation.

REFERENCES

Baldwin, J. M. 1993. The probable arrangement of the helices in G protein-coupled receptors. *EMBO J.* 12:1693–1703.

Belrhali, H., P. Nollert, A. Royant, C. Menzel, J. P. Rosenbusch, E. M. Landau, and E. Pebay-Peyroula. 1999. Protein, lipid and water organization in bacteriorhodopsin crystals: a molecular view of the purple membrane at 1.9 A resolution. *Struct. Fold. Des.* 7:909–917.

Bouchiat, C., M. D. Wang, J-F. Allemand, T. Strick, S. M. Block, and V. Croquette. 1999. Estimating the persistence length of a worm-like chain molecule from force-extension measurements. *Biophys. J.* 76:409–412.

Brooks, C. L., M. Grueberle, J. N. Onuchic, and P. G. Wolynes. 1998. Chemical physics of protein folding. *Proc. Natl. Acad. Sci. U.S.A.* 95:11037–11038.

Bustamante, C., S. B. Smith, J. Liphardt, and D. Smith. 2000. Single-molecule studies of DNA mechanics. *Curr. Opin. Struct. Biol.* 10: 279–285.

Butt, H. J., K. Fendler, E. Bamberg, J. Tittor, and D. Oesterhelt. 1989. Aspartic acids 96 and 85 play a central role in the function of bacteriorhodopsin as a proton pump. *EMBO J.* 8:1657–1663.

Butt, H-J., and M. Jaschke. 1995. Calculation of thermal noise in atomic force microscopy. *Nanotechnology.* 6:1–7.

Clausen-Schaumann, H., M. Seitz, R. Krautbauer, and H. Gaub. 2000. Force spectroscopy with single bio-molecules. *Curr. Opin. Chem. Biol.* 4:524–530.

Dammer, U., M. Hegner, D. Anselmetti, P. Wagner, M. Dreier, W. Huber, and H. J. Güntherodt. 1996. Specific antigen/antibody interactions measured by force microscopy. *Biophys. J.* 70:2437–2441.

Essen, L-O., R. Siegert, W. D. Lehmann, and D. Oesterhelt. 1998. Lipid patches in membrane protein oligomers: Crystal structure of the bacteriorhodopsin-lipid complex. *Proc. Natl. Acad. Sci. U.S.A.* 95: 11673–11678.

Fisher, T. E., A. F. Oberhauser, M. Carrion-Vazquez, P. E. Marszalek, and J. M. Fernandez. 1999. The study of protein mechanics with the atomic force microscope. *Trends Biochem. Sci.* 24:379–384.

Florin, E. L., M. Rief, H. Lehmann, M. Ludwig, C. Dornmair, V. T. Moy, and H. Gaub. 1995. Sensing specific molecular interactions with the atomic force microscope. *Biosens. Biolelectron.* 10:895–901.

Forbes, J. G., and G. H. Lorimer. 2000. Unravelling a membrane protein. *Science.* 288:63–64.

Fritz, J., A. G. Katopodis, F. Kolbinger, and D. Anselmetti. 1998. Force-mediated kinetics of single P-selectin/ligand complexes observed by atomic force microscopy. *Proc. Natl. Acad. Sci. U.S.A.* 95:12283–12288.

Grandbois, M., M. Beyer, M. Rief, H. Clausen-Schaumann, and H. E. Gaub. 1999. How strong is a covalent bond? *Science.* 283:1727–1730.

Grigorieff, N., T. A. Ceska, K. H. Downing, J. M. Baldwin, and R. Henderson. 1996. Electron-crystallographic refinement of the structure of bacteriorhodopsin. *J. Mol. Biol.* 259:393–421.

Haltia, T., and E. Freire. 1995. Forces and factors that contribute to the structural stability of membrane proteins. *BBA Bioenerg.* 1228:1–27.

Haupts, U., J. Tittor, and D. Oesterhelt. 1999. Closing in on bacteriorhodopsin: progress in understanding the molecule. *Annu. Rev. Biophys. Biomol. Struct.* 28:367–399.

Helmreich, E. J. M., and K-P. Hofmann. 1996. Structure and function of proteins in G-protein coupled signal transfer. *Biochem. Biophys. Acta.* 1286:285–322.

Heymann, B., and H. Grubmüller. 2000. Dynamic force spectroscopy of molecular adhesion bonds. *Phys. Rev. Lett.* 84:6126–6129.

Holz, M., Drachev, L. A., Mogi, T., Otto, H., Kaulen, A. D., Heyn, M. P., Skulachev, V. P., Khorana, H. G. 1989. Replacement of aspartic acid-96 by asparagine in bacteriorhodopsin slows both the decay of the M intermediate and the associated proton movement. *Proc. Natl. Acad. Sci. U.S.A.* 86:2167–2171.

Katragadda, M., J. L. Alderfer, and P. L. Yeagle. 2000. Solution structure of the loops of bacteriorhodopsin closely resembles the crystal structure. *Biochim. Biophys. Acta.* 1466:1–6.

Kellermayer, M. S., S. B. Smith, H. L. Granzier, and C. Bustamante. 1997. Folding-unfolding transitions in single titin molecules characterized with laser tweezers. *Science.* 276:1112–1116.

Kolbe, M., H. Besir, L. O. Essen, and D. Oesterhelt. 2000. Structure of the light-driven chloride pump halorhodopsin at 1.8 Å resolution. *Science.* 288:1390–1396.

Lanyi, J. K. 1999. Progress toward an explicit mechanistic model for the light-driven pump, bacteriorhodopsin. *FEBS Lett.* 464:103–107.

Lee, G. U., D. A. Kidwell, and R. J. Colton. 1994. Sensing discrete streptavidin-biotin interactions with atomic force microscopy. *Langmuir.* 10:354–357.

Luecke, H., B. Schobert, H. T. Richter, J. P. Cartailler, and J. K. Lanyi. 1999. Structure of bacteriorhodopsin at 1.55 Å resolution. *J. Mol. Biol.* 291:899–911.

Marszalek, P. E., H. Lu, H. Li, M. Carrion-Vazquez, A. F. Oberhauser, K. Schulten, and J. M. Fernandez. 1999. Mechanical unfolding intermediates in titin modules. *Nature.* 402:100–103.

Merkel, R. 2001. Force spectroscopy on single passive biomolecules and single biomolecular bonds. *Phys. Rep.* 346:343–385.

Merkel, R., P. Nassoy, A. Leung, K. Ritchie, and E. Evans. 1999. Energy landscapes of receptor-ligand bonds explored with dynamic force microscopy. *Nature.* 397:50–53.

Mitsuoka, K., T. Hirai, K. Murata, A. Miyazawa, A. Kidera, Y. Kimura, and Y. Fujiyoshi. 1999. The structure of bacteriorhodopsin at 3.0 Å resolution based on electron crystallography: implication of the charge distribution. *J. Mol. Biol.* 286:861–882.

Möller, C., G. Büldt, N. Dencher, A. Engel, and D. J. Müller. 2000. Reversible loss of crystallinity on photobleaching purple membrane in presence of hydroxylamine. *J. Mol. Biol.* 301:869–879.

Moy, V. T., E-L. Florin, and H. E. Gaub. 1994. Intermolecular forces and energies between ligands and receptors. *Science.* 266:257–259.

Müller, D. J., M. Amrein, and A. Engel. 1997. Adsorption of biological molecules to a solid support for scanning probe microscopy. *J. Struct. Biol.* 119:172–188.

Müller, D. J., D. Fotiadis, S. Scheuring, S. A. Müller, and A. Engel. 1999a. Electrostatically balanced subnanometer imaging of biological specimens by atomic force microscopy. *Biophys. J.* 76:1101–1111.

Müller, D. J., H-J. Sass, S. Müller, G. Büldt, and A. Engel. 1999b. Surface structures of native bacteriorhodopsin depend on the molecular packing arrangement in the membrane. *J. Mol. Biol.* 285:1903–1909.

Nakamara, H. 1996. Roles of electrostatic interaction in proteins. *Q. Rev. Biophys.* 29:1–90.

Oberhauser, A. F., P. E. Marszalek, M. Carrion-Vazquez, and J. M. Fernandez. 1999. Single protein misfolding events captured by atomic force microscopy. *Nat. Struct. Biol.* 6:1025–1028.

Oberhauser, A. F., P. E. Marszalek, H. P. Erickson, and J. M. Fernandez. 1998. The molecular elasticity of the extracellular matrix protein tenascin. *Nature.* 393:181–185.

Oesterhelt, D. 1998. The structure and mechanism of the family of retinal proteins from halophilic archaea. *Curr. Opin. Struct. Biol.* 8:489–500.

Oesterhelt, F., D. Oesterhelt, M. Pfeiffer, A. Engel, H. E. Gaub, and D. J. Müller. 2000. Unfolding pathways of individual bacteriorhodopsins. *Science.* 288:143–146.

Oesterhelt, F., M. Rief, and H. E. Gaub. 1999. Single molecule force spectroscopy by AFM indicates helical structure of poly(ethyleneglycol) in water. *N. J. Phys.* 1:6.1–6.11.

Oesterhelt, D., L. Schuhmann, and H. Gruber. 1974. Light-dependent reaction of bacteriorhodopsin with hydroxylamine in cell suspensions of *Halobacterium halobium*: demonstration of an apo-membrane. *FEBS Lett.* 44:257–261.

Oesterhelt, D., and W. Stoeckenius. 1974. Isolation of the cell membrane of *Halobacterium halobium* and its fraction into red and purple membrane. *Methods Enzymol.* 31:667–678.

Palczewski, K., T. Kumasaka, T. Hori, C. A. Behnke, H. Motoshima, B. A. Fox, I. Le Trong, D. C. Teller, T. Okada, R. E. Stenkamp, M. Yamamoto, and M. Miyano. 2000. Crystal structure of rhodopsin: a G protein-coupled receptor. *Science* 289:739–45.

Pfeiffer, M., T. Rink, K. Gerwert, D. Oesterhelt, and H-J. Steinhoff. 1999. Site-directed spin-labelling reveals the orientation of the amino acid side-chains in the E-F loop of bacteriorhodopsin. *J. Mol. Biol.* 287: 163–171.

Rief, M., H. Clausen-Schaumann, and H. Gaub. 1999. Sequence-dependent mechanics of single DNA molecules. *Nat. Struct. Biol.* 6:346–349.

Rief, M., J. M. Fernandez, and H. E. Gaub. 1998a. Elastically coupled two-level systems as a model for biopolymer extensibility. *Phys. Rev. Lett.* 81:4764–4767.

Rief, M., M. Gautel, and H. E. Gaub. 2000. Unfolding forces of titin and fibronectin domains directly measured by AFM. *Adv. Exp. Med. Biol.* 481:129–136.

Rief, M., M. Gautel, F. Oesterhelt, J. M. Fernandez, and H. E. Gaub. 1997a. Reversible unfolding of individual titin immunoglobulin domains by AFM. *Science.* 276:1109–1112.

Rief, M., M. Gautel, A. Schemmel, and H. E. Gaub. 1998b. The mechanical stability of immunoglobulin and fibronectin III domains in the muscle protein titin measured by AFM. *Biophys. J.* 75:3008–3014.

Rief, M., F. Oesterhelt, B. Heymann, and H. E. Gaub. 1997b. Single molecule force spectroscopy on polysaccharides by AFM. *Science.* 275:1295–1298.

Royant, A., P. Nollert, K. Edman, R. Neutze, E. M. Landau, E. Pebay-Peyroula, and J. Navarro. 2001. X-ray structure of sensory rhodopsin II at 2.1-Å resolution. *Proc. Natl. Acad. Sci. U.S.A.* 98:10131–10136.

Sackmann, E. 1996. Supported membranes: scientific and practical applications. *Science.* 271:43–48.

White, S. H., and W. C. Wimley. 1999. Membrane protein folding and stability: physical principles. *Annu. Rev. Biophys. Biomol. Struct.* 28: 319–365.

Zhang, B., G. Xu, and J. Evans. 1999. A kinetic molecular model of the reversible unfolding and refolding of titin under force extension. *Biophys. J.* 77:1306–1315.